Applied Catalysis B: Environmental 100 (2010) 378–385

Contents lists available at ScienceDirect

Applied Catalysis B: Environmental

journal homepage: www.elsevier.com/locate/apcatb

Study on the shape control and photocatalytic activity of high-energy anatase titania

Zhouyou Wang[a], Kangle Lv[a,b,*], Guanghui Wang[c], Kejian Deng[a], Dingguo Tang[a]

[a] Key Laboratory of Catalysis and Materials Science of the State Ethnic Affairs Commission & Ministry of Education, South-Central University for Nationalities, Wuhan 430074, China
[b] State Key Laboratory of Advanced Technology for Materials Synthesis and Processing, Wuhan University of Technology, Wuhan 430070, China
[c] Hubei Provincial Key Laboratory of Coal Conversion & New Carbon Materials, Wuhan University of Science & Technology, Wuhan 430081, China

ARTICLE INFO

Article history:
Received 24 April 2010
Received in revised form 11 August 2010
Accepted 13 August 2010
Available online 19 August 2010

Keywords:
Titania
Fluoride
Photocatalysis
Photoluminescence
High-energy facet

ABSTRACT

In the present work, high-energy TiO_2 photocatalysts with exposed {0 0 1} facets were tailored by hydrothermal reaction of tetrabutyl titanate (50 g) and HF solution at 200 °C for 24 h. The photocatalysts were characterized by X-ray diffraction, transmission electron microscopy, scanning electron microscopy, nitrogen adsorption–desorption isotherms and X-ray photoelectron spectroscopy. The photocatalytic activity of the photocatalyst was evaluated by a photoluminescence technique using coumarin as a probe molecule. It shows that, with increase in the amount of HF, the shape of TiO_2 evolves from octahedral bipyramid to nanosheet and the percentage of exposed high-energy {0 0 1} facets increases. The photocatalytic activity of the as-prepared high-energy anatase nanocrystals is positively related to the percentage of exposed {0 0 1} facets. When the amount of HF is more than 12 mL, the photocatalytic activity of anatase TiO_2 nanosheets is high than that of P25. The high photocatalytic activity of the high-energy anatase TiO_2 nanocrystals is ascribed to the synergetic effect of exposed high reactive {0 0 1} facets and surface fluorination. However, high concentrated HF (20 mL) results in the formation of cubic $TiOF_2$, which shows very poor photocatalytic activity.

1. Introduction

Oxide semiconductor-mediated photocatalytic purification of polluted air and wastewater is a promising environmental remediation technology, especially for low levels of organic contaminants. Among which, TiO_2 photocatalysis has attracted increasing attention due to its biological and chemical inertness, strong photo oxidization power, cost effectiveness, and long-term stability against photo and chemical corrosion [1–8]. However, a vital problem, i.e., low quantum efficiency, hampers its widespread practical applications. Therefore, the photocatalytic activity of TiO_2 need to be further improved [9–14].

It is often observed that efficiency of organic degradation is a function of physical parameters of TiO_2, such as the crystalline phase, crystallinity, particle size, surface area, specific surfaces and growth orientation of TiO_2 nanocrystals [5,7,8,12,15–23]. Most available anatase TiO_2 crystals are dominated by the thermodynamically stable {1 0 1} facets, rather than the much more reactive {0 0 1} and {0 1 0} facets [22,24]. Recently, an important breakthrough in preparation of anatase TiO_2 crystals with exposed {0 0 1} facets was achieved by Lu and co-workers. They reported the synthesis of anatase TiO_2 microcrystals with 47% {0 0 1} facets on the surface by reversing the relative stability of {1 0 1} and {0 0 1} facets using HF as morphology-controlling agent [4,24]. Now much attention has been paid on the controllable synthesis of nanocrystalline TiO_2 with a large percentage of reactive facets, such as {0 0 1} [4,18,22,25–27], {0 1 0} [22] and {1 1 0} [25] facets. The study of Matsumura [5] and Ohno [23] showed that different surface energy levels of the conduction and valence bands are expected for different crystal facets of TiO_2 because of the atomic arrangements characteristic of these facets. The difference in the energy levels drives the electrons and holes to different crystal faces, leading to separation of electrons and holes, which is very important to the enhancement of the photocatalytic activity. Therefore, it is likely to optimize the photocatalytic activity of anatase TiO_2 by tailoring the exposed high-energy facets.

In this article, anatase TiO_2 nanocrystals with exposed high-energy {0 0 1} facets were tailored using HF as morphology-controlling agent. The relationship between photocatalytic activity and the percentage of exposed {0 0 1} facets of high-energy anatase TiO_2 nanocrystals was studied by a photoluminescence

* Corresponding author at: Key Laboratory of Catalysis and Materials Science of the State Ethnic Affairs Commission & Ministry of Education, South-Central University for Nationalities, Wuhan 430074, China. Tel.: +86 27 67842752; fax: +86 27 67842752.
E-mail address: lvkangle@mail.scuec.edu.cn (K. Lv).

0926-3373/$ – see front matter © 2010 Elsevier B.V. All rights reserved.
doi:10.1016/j.apcatb.2010.08.014

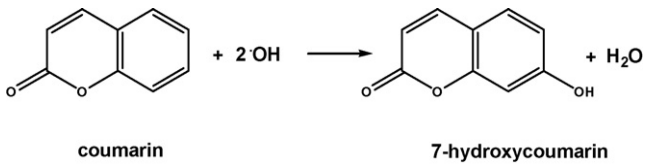

Scheme 1. Formation of 7-hydroxycoumarin in the reaction of coumarin with hydroxyl radicals.

(PL) technique using coumarin as a probe molecule (Scheme 1) [28,29].

2. Experimental

2.1. Sample preparation

Certain amount of HF solution and/or water were dropwise added into 50 g of tetrabutyl titanate (TBT) under magnetic stirring (Table 1). The resulted mixed solution was then transfered to a dried 100-mL Teflon-lined autoclave and kept at 200 °C for 24 h. It should be noted that, hydrofluoric acid is extremely corrosive and it should be handled with extremely care! After being cooled to room temperature, the precipitates were filtrated through a membrane filter (pore size, 0.45 μm), and thoroughly rinsed with distilled water until the pH value of the filtrate is about 7. Then the precipitates were dried in a vacuum oven at 80 °C for 10 h. The resulted sample is denoted as HF*x*, where *x* represents the volumes of HF added into the mixed solution (Table 1).

2.2. Characterization

The X-ray diffraction (XRD) patterns obtained on a D8-advance X-ray diffractometer (German Bruker) using Cu Kα radiation at a scan rate of 0.02° $2\theta\,s^{-1}$ were used to determine the crystalline size and identity. The accelerated voltage and applied current were 15 kV and 20 mA, respectively. The average crystalline size of the catalyst was determined according to the Scherrer equation using full width at half maximum data after correcting for the instrumental broadening. The BET surface area (S_{BET}) of the powders was analyzed by using nitrogen adsorption in a nitrogen-adsorption apparatus (Micromeritics ASAP 2020, USA). The BET surface area was determined by a multipoint BET method using the adsorption data in the relative pressure (P/P_0) range of 0.05–0.3. Pore volume and average pore size were determined by nitrogen-adsorption volume at the relative pressure of 0.994. All the samples were degassed at 180 °C prior to the nitrogen-adsorption measurements. The morphology of the photocatalyst was observed on a transmission electron microscopy (TEM) (Tecnai G20, USA) using an acceleration voltage of 200 kV and a field emission scanning electron microscope (SEM) (Hitach, Japan) with an acceleration voltage of 20 kV, respectively. X-ray photoelectron spectroscopy (XPS) measurements were done with a Kratos XSAM800 XPS system with Mg Kα source and a charge neutralizer, all the binding energies were referenced to the C 1s peak at 284.8 eV of the surface adventitious carbon.

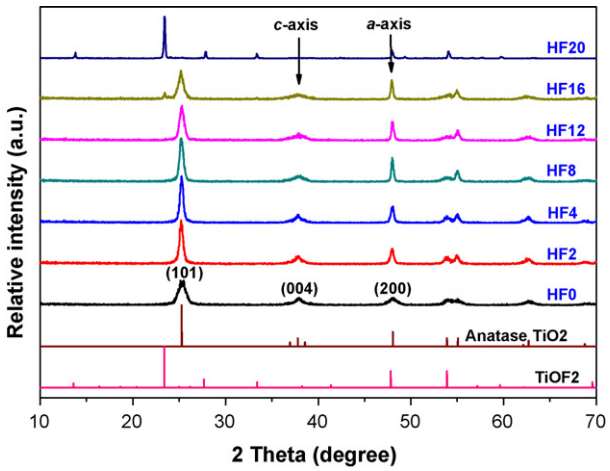

Fig. 1. XRD patterns of the photocatalysts, together with the expected diffraction peaks for anatase TiO_2 and $TiOF_2$.

2.3. Photocatalytic activity

The photocatalytic activity of the photocatalyst was evaluated by a photoluminescence (PL) technique using coumarin as a probe molecule, which readily reacted with •OH radicals to produce highly fluorescent product, 7-hydroxycoumarin (Scheme 1) [29,30]. The suspensions of TiO_2 (1.0 g/L) containing coumarin (0.5 mmol/L) is mixed under magnetic stirring, and then was shaken overnight. At given intervals of irradiation, small aliquots were withdrawn by a syringe, and filtered through a membrane (pore size 0.45 μm). The filtrate was analyzed on a Hitachi F-7000 fluorescence spectrophotometer by the excitation with the wavelength of 332 nm.

3. Results and discussion

3.1. Crystal structure and morphology

The phase structure, crystalline size and shape (or facets exposed on the surface) of TiO_2 are of great importance for its photocatalytic activity [8,31]. Fig. 1 shows the XRD patterns of the photocatalysts. A broad peak at $2\theta = 25.3°$ corresponding to the (1 0 1) plane diffraction of anatase TiO_2 (JCPDS No. 21-1272) [32,33] was observed for HF0 sample. The broadening of the diffraction peak is caused by weak crystallization of the sample. With increasing the amount of HF to 2 and 4 mL, the peak intensities of anatase increase, indicating an enhancement of crystallization, which is concord with the report of Yu et al. that fluoride enhances the crystallinity of anatase [34]. It was reported that the presence of fluoride ions at low pH accelerates TiO_2 crystallization and growth

Table 1
Physical properties of the photocatalysts.

Catalyst	Materials			Characterization results			
	$Ti(OC_4H_9)_4$ (g)	HF (mL)	H_2O (mL)	Percentage of {0 0 1} facets	S_{BET} (m^2/g)	Pore volume (cm^3/g)	Ave. pore size (nm)
HF0	50	0	8	6	138	0.31	8.8
HF2	50	2	6	41	82	0.26	10.0
HF4	50	4	4	63	74	0.23	11.9
HF8	50	8	0	88	63	0.43	24.1
HF12	50	12	0	93	45	0.25	19.2
HF16	50	16	0	96	36	0.14	15.0
HF20	50	20	0	–	9.3	0.05	14.5

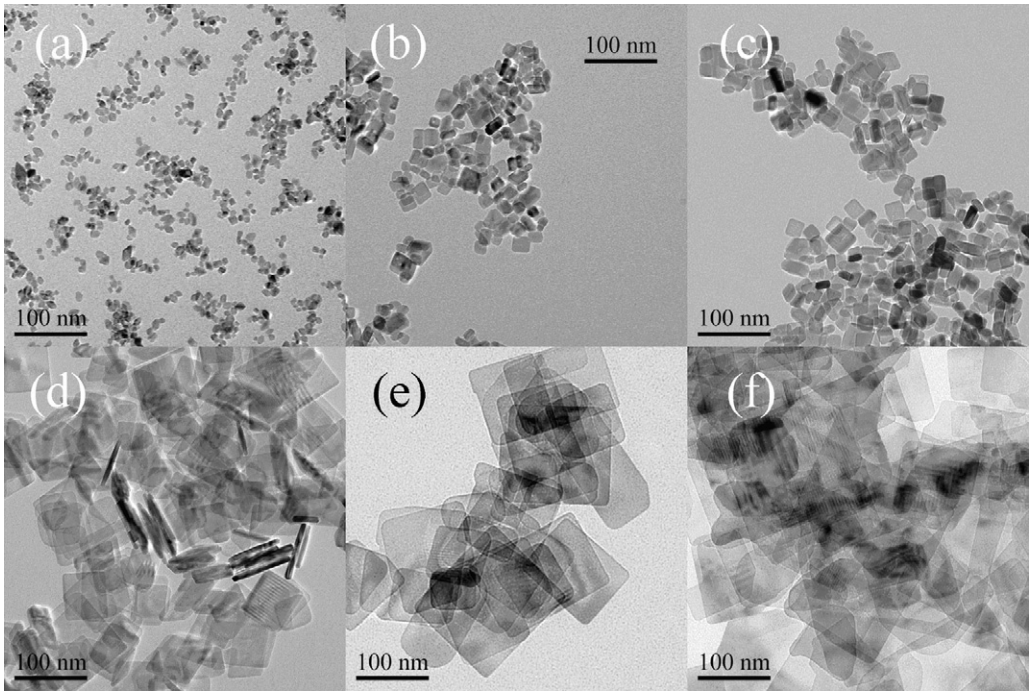

Fig. 2. TEM images of HF0 (a), HF2 (b), HF4 (c), HF8 (d), HF12 (e) and HF16 (f) TiO_2 samples, respectively.

due to rapid *in situ* dissolution–recrystallization, which reduces the numbers of defects and impurities in the TiO_2 lattice (Eqs. (1) and (2)). Therefore, it is understandable of the formation of the well-crystallized anatase TiO_2 single crystals in the presence of HF.

$$4H^+ + TiO_2 + 6F^- \rightarrow TiF_6^{2-} + 2H_2O \quad \text{(dissolution)} \tag{1}$$

$$TiF_6^{2-} + 2H_2O \rightarrow 4H^+ + TiO_2 + 6F^- \quad \text{(recrystallization)} \tag{2}$$

However, with further increase in the amount of HF from 8 to 16 mL, the relative crystallinity of anatase TiO_2 decreases. This is due to the strong affinity of fluoride to titanium, inhibiting the extensive Ti–O–Ti bridging and crystal growth.

When the amount of HF is increased to 20 mL, the peaks of anatase TiO_2 vanish and an obvious peak at $2\theta = 23.4^\circ$, corresponding to the (1 0 0) plane diffraction of $TiOF_2$ (JCPDS No. 01-0490), appears. This reflects that $TiOF_2$ can be formed in high concentrated HF solution.

Figs. 2 and 3 show TEM and high-resolution TEM (HRTEM) images of the photocatalyst, respectively. It can be seen from Fig. 3(a) that anatase HF0 TiO_2 nanocrystals were of octahedral

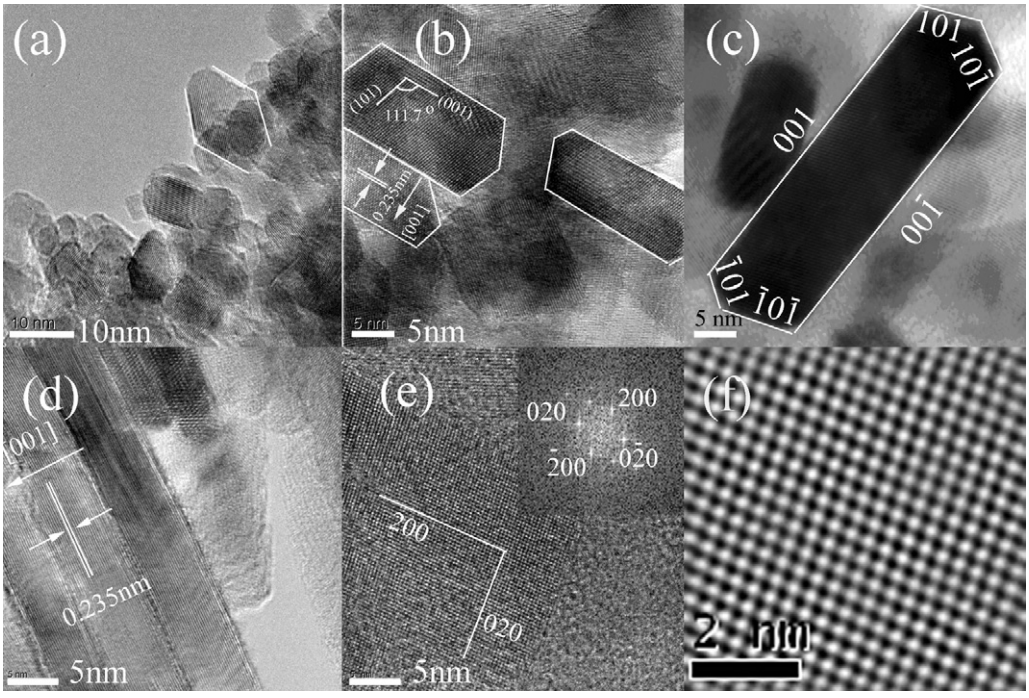

Fig. 3. High-resolution TEM images of HF0 (a), HF2 (b), HF4 (c) and HF8 (d and e) TiO_2 sample, respectively. Inset of (e) is the fast-Fourier transform (FFT) pattern of HF8 indexed to the [0 0 1] zone, and (f) is the corresponding fast-Fourier-transform-filtered TEM image.

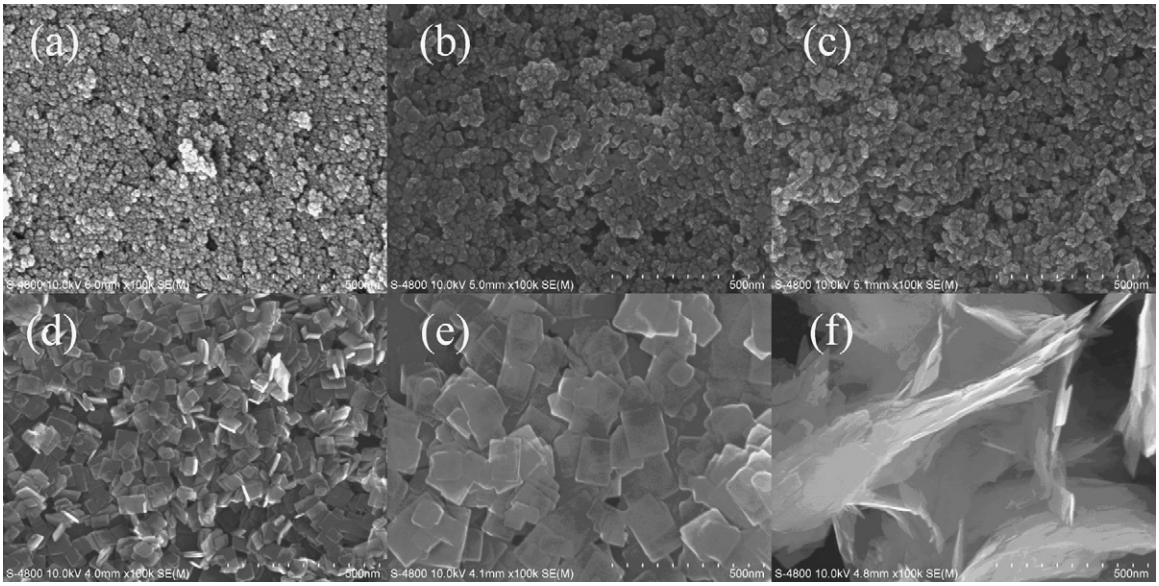

Fig. 4. SEM images of HF0 (a), HF2 (b), HF4 (c) and HF8 (d), HF12 (e), and HF16 (f) TiO_2 samples, respectively.

bipyramidal shape with a width of ca. 10 nm (along the *a*-axis) and a thickness of ca. 15 nm (along the *c*-axis), which is exposed with eight low-energy {1 0 1} facets, similar to the equilibrium shape of anatase crystals predicted by Wulff construction from surface energy calculations (inset of Fig. 5(a)) [8]. This is due to the rapid diminishing of surfaces with high reactivity during the crystal growth process to minimize the surface energy [24].

TEM images of HF2 (Figs. 2(b) and 3(b)) shows that the shape of HF2 evolves into a truncated octahedronal bipyramid. The side view HRTEM image of HF2 shown in Fig. 3 directly shows that the lattice spacing parallel to the top and bottom facets is ca. 0.235 nm, corresponding to the (0 0 1) planes of anatase TiO_2, which indicates the top and bottom facets are the (0 0 1) and (0 0 $\bar{1}$) planes, respectively. An angle of ca. 111.7°, consistent with the interfacial angle between (0 0 1) and (1 0 1), is also observed on the hexagonal-shaped particle of HF2, suggesting that the particle exhibits flat surfaces of (0 0 1) and (1 0 1). Therefore, HF2 is characterized by a truncated octahedronal bipyramid which is enclosed by eight equivalent {1 0 1} facets and two equivalent {0 0 1} facets (inset of Fig. 5(b)). Compared with that of HF0, the width of HF2 increases to ca. 20 nm while the thickness decreases to about 10 nm. Using the Scherrer equation, the average sizes of HF2 along [0 0 1] and [100] directions were calculated to be 12.7 and 21.5 nm, respectively, very close to the results obtained from HRTEM image (Fig. 3(b)). The experimental results reflect that HF2 have the preferential growth along *a*-axis, resulting in the exposure of high-energy {0 0 1} facets in the presence of shape-controlling agent HF.

The shape of HF4 is similar to that of HF2 except in length and thickness (Figs. 2(c) and 3(c)). Fig. 4(a)–(c) shows the SEM images of HF0, HF2 and HF4 TiO_2 nanoparticles, respectively. It can be observed that with increase in the amount of HF solution, the particle sizes of the photocatalysts increase, which is consistent with the observation from TEM (Fig. 2(a)–(c)).

The preferential growth along *a*-axis and the resulting exposure of high-energy {0 0 1} facets can be more clearly observed in HF8 sample, which is consisted of well-defined sheet-shaped struc-

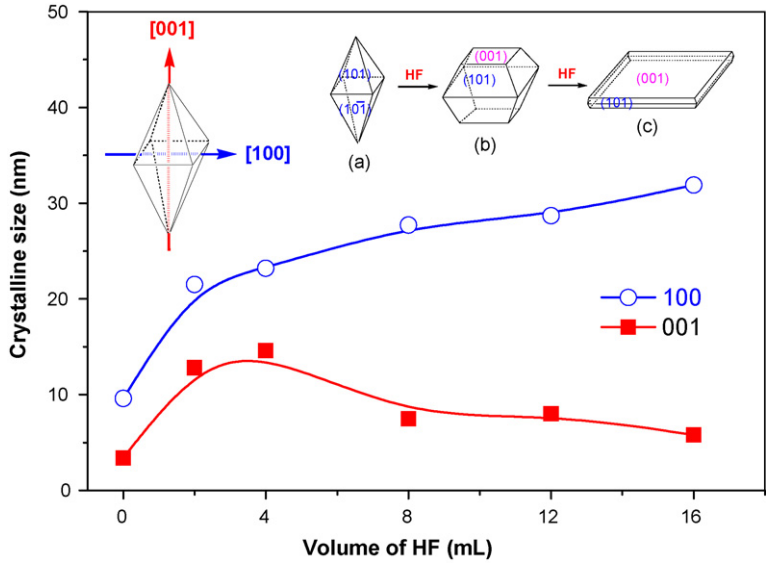

Fig. 5. Dependence of average crystalline sizes of the photocatalysts along [0 0 1] and [100] direction on the amount of HF solution, indicating that the photocatalyst has the preferential growth along *a*-axis, whilst the growth along *c*-axis is restrained (inset is the corresponding shape simulation: octahedral bipyramid (a), truncated octahedral bipyramid (b) and nanosheet (c)).

tures having a rectangular outline, side length of ca. 100 nm, and thickness of ca. 6 nm (Fig. 2(d)). Similar to that of HF2 sample, the side view HRTEM image also directly shows a lattice spacing of ca. 0.235 nm, corresponding to the (0 0 1) planes of anatase TiO_2 (Fig. 3(d)). Fig. 3(e) further shows a HRTEM image of the top view of HF8 nanosheet. The lattice fringes could be indexed into (2 0 0) and (0 2 0) planes *via* measuring the lattice spacing and interfacial angle. The corresponding fast-Fourier transform (FFT) pattern of HF8 indexed to the [0 0 1] zone also indicates that the top and bottom facets of the nanosheets were the (0 0 1) planes (inset of Fig. 3(e) and (f)). On the basis of the above structural information, the percentage of highly reactive {0 0 1} facets in HF8 is estimated to be about 88%.

With further increase in the amount of HF solution, the side length of TiO_2 nanosheet further increases, whilst the thickness decreases. The average side length of HF12 and HF16 increases to ca. 130 and 200 nm, but the thickness decreases to about 5 and 4 nm, respectively (Figs. 2 and 4). The perecentages of exposed {0 0 1} facets for HF12 and HF16 are calculated to increase to 93% and 96%, respectively. According to the theory estimation and experimental results, the percentage of exposed {0 0 1} facets for the TiO_2 nanoparticles is less than 10% (ca. 6% for HF0) [35]. Therefore, it can be concluded that the presence of fluoride facilitates the exposure of high-energy {0 0 1} facets of anatase TiO_2, which enhances the growth of anatase TiO_2 nancrystals along the *a*-axis while restricts the growth along the *c*-axis (inset in Fig. 5).

Fig. 5 shows the relationship between average crystalline sizes of the photocatalysts (along [1 0 0] and [0 0 1] directions) and the amount of HF solution used. It can be seen that the crystalline sizes along [1 0 0] direction steadily increase with increasing the amount of HF, but the crystalline sizes along [0 0 1] direction increase first and then decrease, which further confirms the preferential growth of high-energy anatase TiO_2 nanocrystals along *a*-axis in the presence of the HF (inset of Fig. 5). The fact that the crystalline sizes of the photocatalyst along [0 0 1] direction increase with increasing the amount of HF (0–4 mL) at first is due to fluoride induced enhancement of crystallinity (Eqs. (1) and (2)). Note that the average crystalline sizes of the high-energy anatase TiO_2 nanocrystals along [1 0 0] direction is smaller than these observed by SEM and TEM images when the amount of HF is high than 8 mL. This is due to the weak crystallinity of the photocatalyst in high concentrated HF solution (Fig. 1).

The average surface energy for {0 0 1} facets is calculated to be 0.90 J/m^2, much higher than that of {1 0 1} facets (0.44 J/m^2). Therefore, most available anatase TiO_2 crystals are dominated by the thermodynamically stable {1 0 1} facets (more than 94%, according to the Wulff construction), rather than the much more reactive {0 0 1} facets [24]. However, due to the strong electronegativity of the fluorine atoms and high binding energies of Ti–F (569.0 kJ/mol), a new balance between O–O/F–O repulsions and Ti–O/Ti–F attractions can be constructed on the surface of anatase TiO_2 in the presence of HF, which stabilize Ti and O atoms on the surface. In the case of clean surfaces, the adsorption energy of F over (0 0 1) and (1 0 1) is 4.4 and 2.8 eV, respectively [4]. Then the relative stability is reversed: {0 0 1} is energetically preferable to {1 0 1} for fluorine-terminated TiO_2 surfaces, which results in the preferential adsorption of fluorine on the (0 0 1) surface, restricting the growth of anatase TiO_2 nanocrystals along the *c*-axis [24]. Therefore, anatase TiO_2 nanosheets with a high percentage of reactive {0 0 1} facets can be obtained using HF as a structure-directing agent [35]. Inset of Fig. 5 illustrates the effect of HF on the shape control of anatase TiO_2 nanocrystals. Note that no anatase TiO_2 but cubic $TiOF_2$ is obtained when the amount of HF further increases to 20 mL due to the high concentrated HF (Figs. 1 and 6).

3.2. BET surface areas and pore size distributions

Fig. 7(A) shows nitrogen adsorption–desorption isotherms and the corresponding pore size distribution curves of the photocatalyst. It can be seen that the isotherm of HF0 is type IV and one hysteresis loop at a relative pressure range of 0.6–0.9, indicating the presence of mesopores (type H2), which can be observed in the ink-

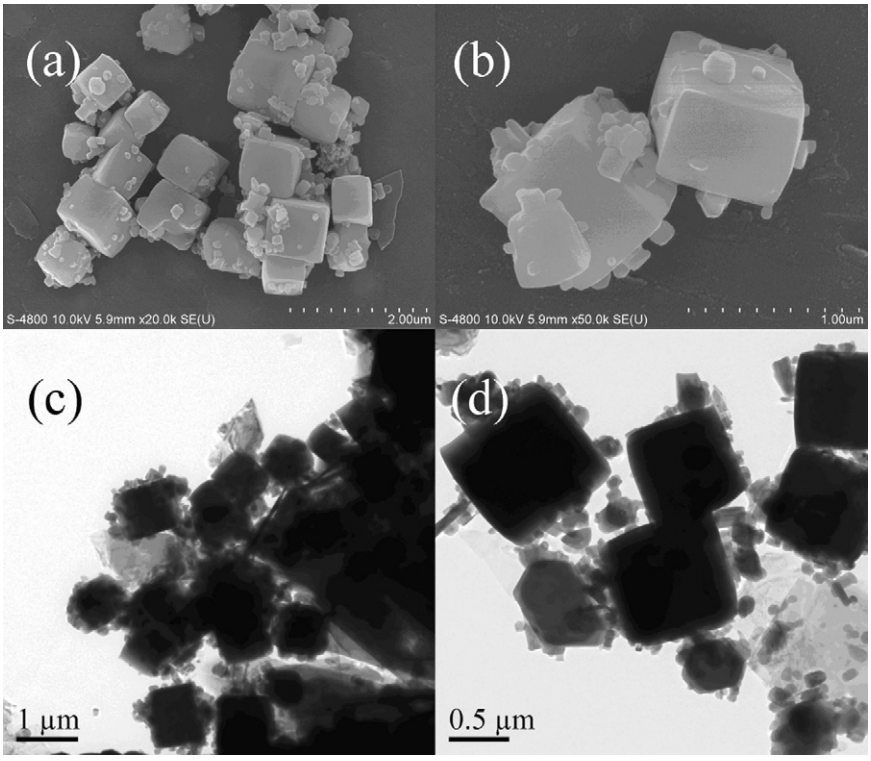

Fig. 6. SEM (a and b) and TEM (c and d) images of HF20 TiO_2 sample.

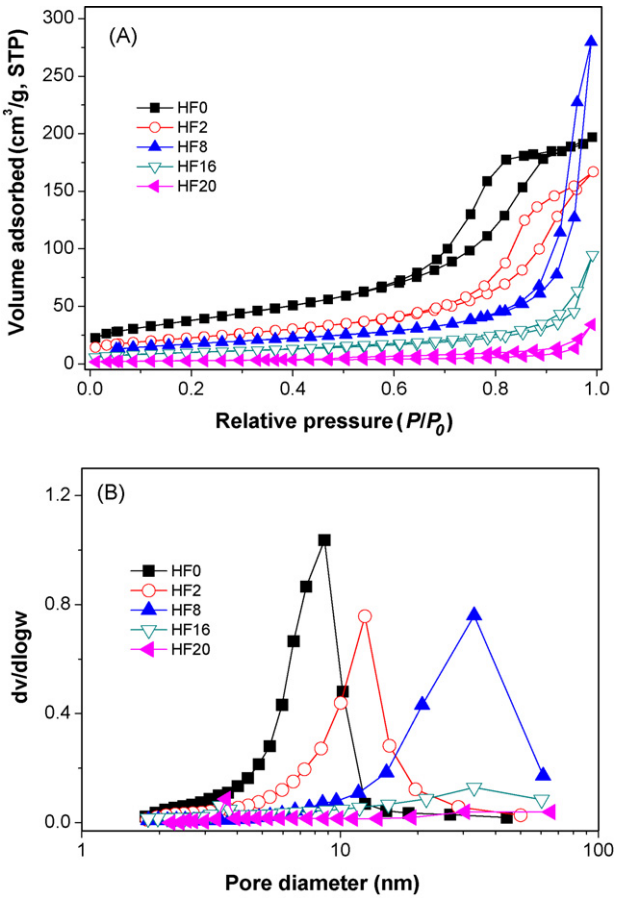

Fig. 7. Nitrogen sorption–desorption isotherms (A) and the corresponding pore size distributions of the photocatalysts (B).

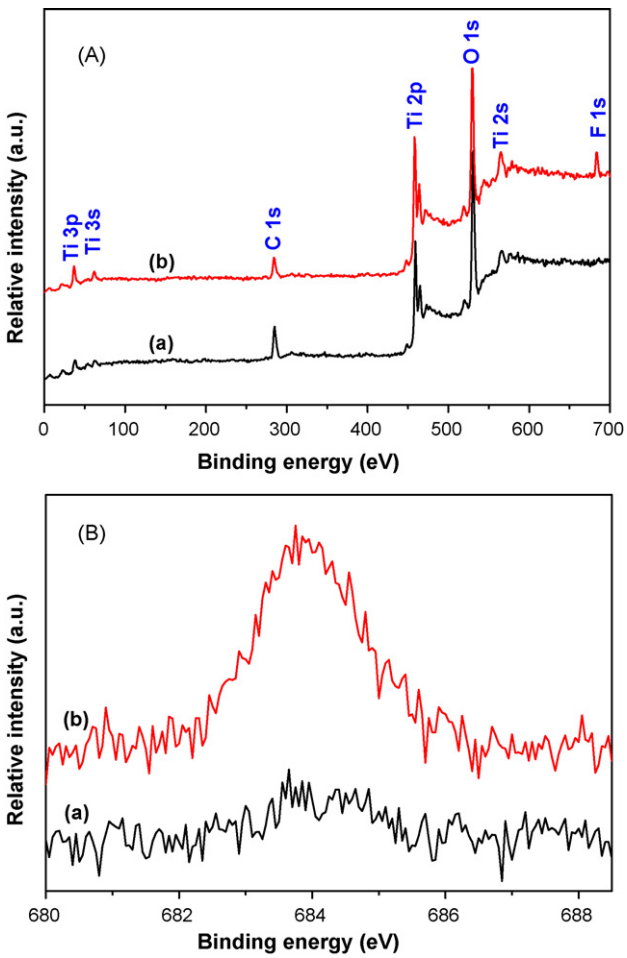

Fig. 8. XPS survey spectra (A) and the corresponding high-resolution XPS spectra of F 1s (B) of HF0 (a) and HF8 (b), respectively.

bottle-like pores with narrow necks and wider bodies [11]. These mesopores are from the aggregation of primary particles (Fig. 4(a)). However, with increase in the amount of HF from 2 to 8 mL, the adsorption isotherms shift downward and the hysteresis loops also move to a relative high pressure range, indicating the decrease of specific BET surface areas and the increase of average pore sizes (Fig. 7(B)). Typically, the shapes of the hysteresis loop for HF8 TiO_2 powders become type H3 [36], suggesting narrow slit-shaped pores that are generally associated with plate-like particles, which agrees well with their sheet-like morphology (Figs. 2(d) and 4(d)). Further increase in the amount of HF, the hysteresis loop diminishes due to the growth of anatase TiO_2 nanosheets and the formation of large cubic $TiOF_2$ microcrystals (Figs. 4(d)–(f) and 6).

Table 1 summarizes the physical properties of the photocatalysts. It can be seen that the BET specific surface areas steadily decrease (from 138 to 36 m^2/g) with increasing the amount of HF solution. Note that the average pore sizes of TiO_2 nanosheets (24.1 nm such as HF8) is less than the average side length (100 nm such as HF8). This is due to the fact that these nanosheets are not individually dispersed and easily connected with each other along [0 0 1] direction (Fig. 3(d)) to minimize the surface energy. HF20 shows the smallest BET specific surface areas (only 9.3 m^2/g) due to the formation of cubic $TiOF_2$, which is similar to the report in literature [37].

3.3. XPS analysis

Fig. 8(A) shows the typical XPS survey spectra of the naked (HF0) and fluorinated TiO_2 (HF8) sample, respectively. It can be seen that HF0 only contains Ti, O and C elements, with sharp photoelectron peaks appearing at binding energies of 459 (Ti 2p), 530 (O 1s) and 285 eV (C 1s), respectively [38,39]. The carbon peak is attributed to the residual carbon from the sample and adventitious hydrocarbon from XPS instrument itself. As expected, an additional peak at 684 eV (F 1s) is found in the survey spectrum of HF8 sample.

$$\equiv Ti{-}OH + HF \rightarrow \equiv Ti{-}F + H_2O \quad (3)$$

The F 1s binding energy peak (Fig. 8(B)) originates from surface fluoride (≡Ti–F) formed by ligand exchange between F^- and surface hydroxyl groups (Eq. (3)) [24,27,34,40]. No signal for F^- in the lattice of TiO_2 (binding energy of 688.5 eV) [34] is found in all the photocatalysts. This is not difficult to understand because, on the one hand, the hydrothermal environment can accelerate crystallization of TiO_2 due to the in situ dissolution–recrystallization process, resulting in the reduction of the number of defects and impurity in TiO_2 crystals (Eqs. (1) and (2)). The actual amount of fluorine detected by XPS slightly increases with increase the amount of HF (from 4.58 to 6.09 at.% for HF2 and HF8 sample, respectively) due to the saturation adsorption of F^- on the TiO_2 surface (Eq. (3)).

It is well known that surface fluorination can greatly enhance the photocatalytic activity of anatase TiO_2 since the •OH radicals generated on the surface of F–TiO_2 are more mobile than those generated on pure TiO_2 under UV irradiation (Eqs. (4) and (5)) [2,14].

$$\equiv Ti{-}OH + h_{vb}^+ \rightarrow \equiv Ti{-}OH^{\bullet +} \quad (^{\bullet}OH_{ads}) \quad (4)$$

$$\equiv Ti{-}F + H_2O + h_{vb}^+ \rightarrow \equiv Ti{-}F + {}^{\bullet}OH_{free} + H^+ \quad (5)$$

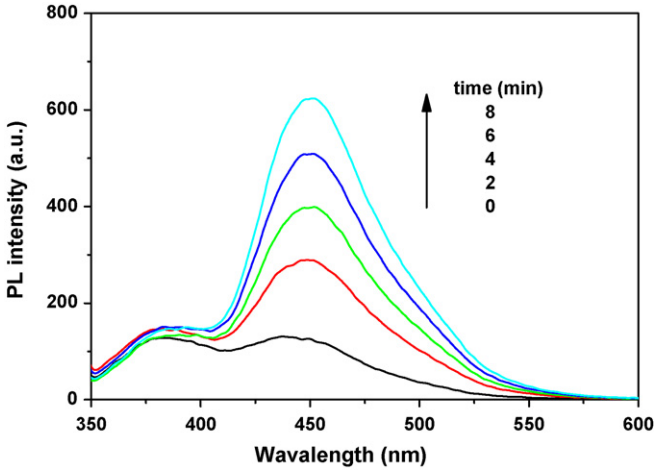

Fig. 9. Photoluminescence spectral changes observed during illumination of the suspensions of HF8 TiO_2 sample.

Therefore, surface fluorinaiton can also enhance the photocatalytic activity of the high-energy TiO_2 nanocrystals, which will be shown below.

3.4. Photocatalytic activity

Recently, it has been proved that several non- or weakly luminescent test molecules, such as terephthalic acid [41–43] and coumarin [29,30,41] produce strongly luminescent compounds with •OH radical, and these molecules can be applied for evaluation of the relative photocatalytic activity of the photocatalyst. Here coumarin is used as a probe to evaluate the photocatalytic activity of high-energy anatase TiO_2 nanocrystals. Fig. 9 shows the typical PL spectral changes observed during illumination of the suspensions of HF8. It is observed that the PL intensity of photo-generated 7-hydroxycoumarin at 450 nm (excited at 332 nm) increases with irradiation time. Fig. 10(A) records the time course of the PL intensity of 7-hydroxycoumarin at 450 nm during the irradiation of the photocatalysts. It is clearly seen that the PL intensity at 450 nm increases linearly against the irradiation time. This leads to a conclusion that the generation of fluorescent 7-hydroxycoumarin is linearly proportional to illumination time, obeying a pseudo-zero-order reaction rate equation in kinetics. The slopes for the curve of PL intensity *versus* illumination time (rate constant), which represent the photocatalytic activity of the photocatalyst, steadily increase with increasing the amount of HF solution. The rate constants for HF12 and HF16 are 79.74 and 95.50, respectively, high than that of Degussa P25 TiO_2 (rate constant of 75.38) (Fig. 10).

Considering that HF serves not only as a structure-directing agent but also results in the surface fluorination (Fig. 8), which can enhance the photocatalytic activity of anatase TiO_2 nanocrystals. To evaluate the effect of adsorbed fluoride ions on the photocatalytic activity of the photocatalyst, photocatalytic activity of the clean (fluorine-free) high-energy TiO_2 nanosheets is also tested. It has been reported that the adsorbed fluorine ions on the surface of TiO_2 can be easily removed by alkaline washing in a NaOH solution without altering the crystal structure and morphology [44]. In this study, the fluorinated TiO_2 nanocrystals were washed using 1 M NaOH solution and distilled water, and then the photocatalytic activity of the treated samples was tested. Experimental results show that the photocatalytic activity of HF8 and HF12 decrease from 60.67 and 95.50 to 29.48 and 44.31, respectively (Fig. 11). It suggests that the photocatalytic activity of fluorine-free high-energy TiO_2 nanocrystals also increases with increasing the percentages of exposed {0 0 1} facets, and surface fluorination plays a positive role

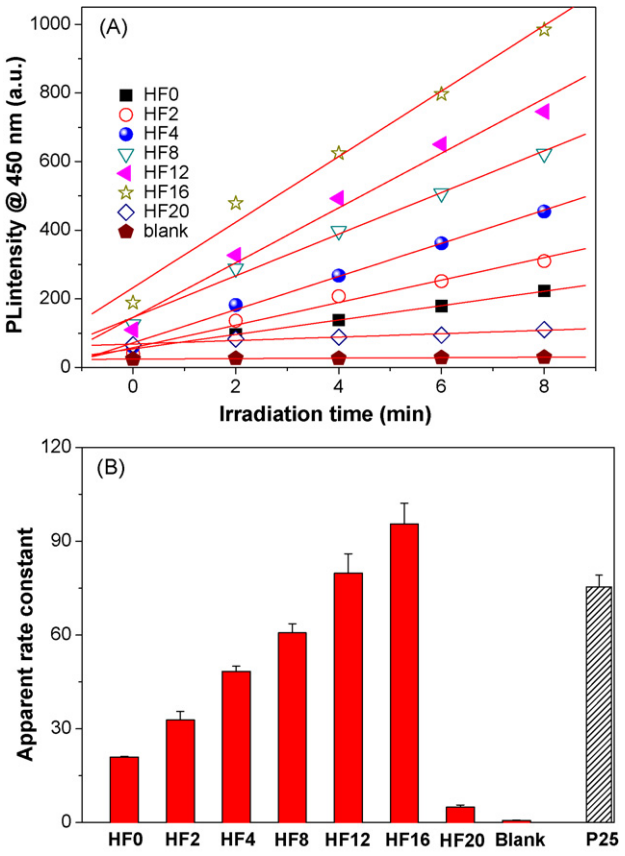

Fig. 10. Time dependence of the induced photoluminescence intensity @ 450 nm of the photocatalysts (A) and comparison of the rate constants (B).

on the enhanced photocatalytic activity. Note that the morphology of the photocatalyst, observed by SEM and TEM images, keeps unchanged after washed by NaOH solution (not shown here).

According to the literatures [5,23], for anatase particles, the oxidation reaction mainly occurs on the {0 0 1} facets and the reduction reaction mainly occurs on the {1 0 1} facets. From the viewpoint of geometry, the sheet-like shape of TiO_2 nanocrystals can facilitate an efficient separation of photo-generated electrons and holes, which is important to the photocatalytic activity of anatase TiO_2 nanocrystals. Theoretical and experimental studies have indicated that the (0 0 1) surface of anatase TiO_2 is much more

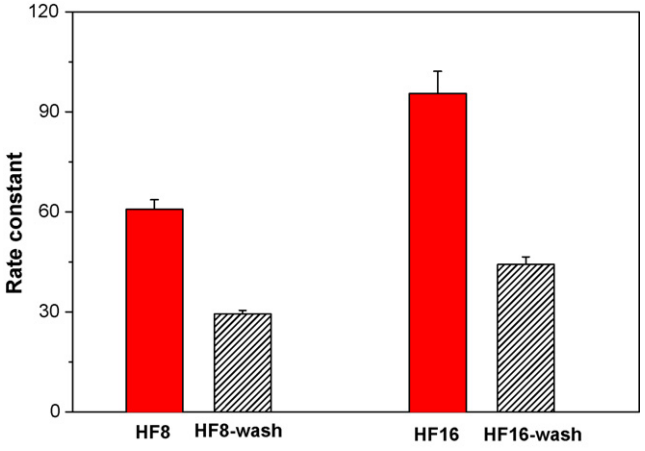

Fig. 11. Comparison of the photocatalytic activity of the photocatalysts before and after washed by 1.0 M NaOH solution.

reactive than the thermodynamically more stable (1 0 1) surface. Therefore, the high photocatalytic activity of the high-energy TiO_2 nanocrystals is ascribed to synergetic effect of the exposed high-energy {0 0 1} facets and surface fluorination.

As expected, HF20 shows poor photocatalytic activity (rate constant of 4.99) due to the formation of non-photoreactive $TiOF_2$. Blank experiment (in the absence of TiO_2) is also performed for comparison, which shows negligible effect on evaluation the photocatalytic activity of the photocatalyst (rate constant of only 0.68).

4. Conclusions

Fluorine plays an important role on microstructure and photocatalytic activity of TiO_2. By reversion the relative stability of low-energy {1 0 1} and high-energy {0 0 1} facets, structure-directing agent HF facilitates the exposure of high-energy {0 0 1} facets, resulting in the formation of sheet-like anatase TiO_2 nanocrystals. The photocatalytic activity of high-energy anatase TiO_2 nanocrystals increases with increasing the amount of HF solution due to the exposed high-energy {0 0 1} facets and surface fluorination. However, $TiOF_2$ is formed in the presence of high concentrated HF, which shows very poor photocatalytic activity. This study may provide new insight into design and preparation of advanced photocatalytic materials.

Acknowledgements

This work was supported by the National Natural Science Foundation of China (20977114), China Postdoctoral Science Foundation (20090451086), Hubei Coal Conversion & New Carbon Materials Key Laboratory (2009WKDM01) and the Knowledge Innovation Program (YZCX100202Z) from South-Central University for Nationalities.

References

[1] T. Miyasaka, N. Ikeda, T.N. Murakami, K. Teshima, Chem. Lett. 36 (2007) 480.
[2] H. Kim, W. Choi, Appl. Catal. B 69 (2007) 127.
[3] M. Lim, Y. Zhou, B. Wood, L.Z. Wang, V. Rudolph, G.Q. Lu, Environ. Sci. Technol. 43 (2009) 538.
[4] H.G. Yang, G. Liu, S.Z. Qiao, C.H. Sun, Y.G. Jin, S.C. Smith, J. Zou, H.M. Cheng, G.Q. Lu, J. Am. Chem. Soc. 131 (2009) 4078.
[5] T. Ohno, K. Sarukawa, M. Matsumura, New J. Chem. 26 (2002) 1167.
[6] P. Periyat, S.C. Pillai, D.E. McCormack, J.C. Colreavy, S.J. Hinder, J. Phys. Chem. C 112 (2008) 7644.
[7] D.H. Wang, J. Liu, Q.S. Huo, Z.M. Nie, W.G. Lu, R.E. Williford, Y.B. Jiang, J. Am. Chem. Soc. 128 (2006) 13670.
[8] Y.Q. Dai, C.M. Cobley, J. Zeng, Y.M. Sun, Y.N. Xia, Nano Lett. 9 (2009) 2455.
[9] X.F. Cheng, W.H. Leng, D.P. Liu, Y.M. Xu, J.Q. Zhang, C.N. Cao, J. Phys. Chem. C 112 (2008) 8725.
[10] M.R. Hoffmann, S.T. Martin, W. Choi, D.W. Bahnemann, Chem. Rev. 95 (1995) 69.
[11] J.G. Yu, W.G. Wang, B. Cheng, B.L. Su, J. Phys. Chem. C 113 (2009) 6743.
[12] K.L. Lv, H.S. Zuo, J. Sun, K.J. Deng, S.C. Liu, X.F. Li, D.Y. Wang, J. Hazard. Mater. 161 (2009) 396.
[13] X.F. Li, K.L. Lv, K.J. Deng, J.F. Tang, R. Su, J. Sun, L.Q. Chen, Mater. Sci. Eng. B 158 (2009) 40.
[14] K.L. Lv, J.G. Yu, K.J. Deng, J. Sun, Y.X. Zhao, D.Y. Du, M. Li, J. Hazard. Mater. 173 (2010) 539.
[15] K.L. Lv, Y.M. Xu, J. Phys. Chem. B 110 (2006) 6204.
[16] Y.M. Xu, K.L. Lv, Z.G. Xiong, W.H. Leng, W.P. Du, D.L. Liu, X.J. Xue, J. Phys. Chem. C 111 (2007) 19024.
[17] K.L. Lv, C.S. Lu, Chem. Eng. Technol. 31 (2008) 1272.
[18] X.Y. Hu, T.C. Zhang, Z. Jin, S.Z. Huang, M. Fang, Y.C. Wu, L.D. Zhang, Cryst. Growth Des. 9 (2009) 2324.
[19] T. Taguchi, Y. Saito, K. Sarukawa, T. Ohnoz, M. Matsumura, New J. Chem. 27 (2003) 1304.
[20] X. Wu, H. Song, J. Yoon, Y. Yu, Y. Chen, Langmuir 25 (2009) 6438.
[21] F. Amano, O. Prieto-Mahaney, Y. Terada, T. Yasumoto, T. Shibayama, B. Ohtani, Chem. Mater. 21 (2009) 2601.
[22] B.H. Wu, C.Y. Guo, N.F. Zheng, Z.X. Xie, G.D. Stucky, J. Am. Chem. Soc. 130 (2008) 17563.
[23] N. Murakami, Y. Kurihara, T. Tsubota, T. Ohno, J. Phys. Chem. C 113 (2009) 3062.
[24] H.G. Yang, C.H. Sun, S.Z. Qiao, J. Zou, G. Liu, S.C. Smith, H.M. Cheng, G.Q. Lu, Nature 453 (2008) 638.
[25] M. Liu, L.Y. Piao, L. Zhao, S. Ju, Z.J. Yan, T. He, C.L. Zhou, W.J. Wang, Chem. Commun. (2010) 1664.
[26] D.Q. Zhang, G.S. Li, X.F. Yang, J.C. Yu, Chem. Commun. (2009) 4381.
[27] J.G. Yu, Q.J. Xiang, J.R. Ran, S. Mann, Appl. Catal. B 96 (2010) 557.
[28] K.L. Lv, X.F. Li, K.J. Deng, J. Sun, X.H. Li, M. Li, Appl. Catal. B 95 (2010) 383.
[29] H.M. Guan, L.H. Zhu, H.H. Zhou, H.Q. Tang, Anal. Chim. Acta 608 (2008) 73.
[30] H. Czili, A. Horvath, Appl. Catal. B 81 (2008) 295.
[31] J.G. Yu, L.J. Zhang, B. Cheng, Y.R. Su, Appl. Catal. B 9 (2010) 214.
[32] J.G. Yu, Y.R. Su, B. Cheng, Adv. Funct. Mater. 17 (2007) 1984.
[33] H.S. Zuo, J. Sun, K.J. Deng, R. Su, F.Y. Wei, D.Y. Wang, Chem. Eng. Technol. 30 (2007) 577.
[34] J.C. Yu, J.G. Yu, W. Ho, Z. Jiang, L.Z. Zhang, Chem. Mater. 14 (2002) 3808.
[35] X.G. Han, Q. Kuang, M.S. Jin, Z.X. Xie, L.S. Zheng, J. Am. Chem. Soc. 131 (2009) 3152.
[36] S.W. Liu, J.G. Yu, J. Solid State Chem. 181 (2008) 1048.
[37] J. Zhu, D.Q. Zhang, Z.F. Bian, G.S. Li, Y.N. Huo, Y.F. Lu, H.X. Li, Chem. Commun. (2009) 5394.
[38] J.G. Yu, M.H. Zhou, B. Cheng, X.J. Zhao, J. Mol. Catal. A 246 (2006) 176.
[39] M.H. Zhou, J.G. Yu, J. Hazard. Mater. 152 (2008) 1229.
[40] H. Park, W. Choi, J. Phys. Chem. B 108 (2004) 4086.
[41] K. Ishibashi, A. Fujishima, T. Watanabe, K. Hashimoto, Electrochem. Commun. 2 (2000) 207.
[42] Q. Xiao, Z.C. Si, J. Zhang, C. Xiao, X.K. Tan, J. Hazard. Mater. 150 (2008) 62.
[43] K.L. Lv, J.G. Yu, K.J. Deng, X.H. Li, M. Li, J. Phys. Chem. Solid 71 (2010) 519.
[44] Q.J. Xiang, K.L. Lv, J.G. Yu, Appl. Catal. B 96 (2010) 557.